Nonmonotonic spatial profiles of excitation rates in bounded plasmas caused by effects of EDF nonlocality

E. A. Bogdanov, A. A. Kudryavtsev and L. D. Tsendin.

***Abstract*— It is shown that the impact of the electron distribution function (EDF) nonlocality on the spatial profiles of excitation rates is important up to high gas pressures pR <100 cmTorr. A paradoxical effect related to the nonlocal character of the EDF is revealed: the peaks of the profiles of the excitation rates shift from the discharge axis toward the periphery as the pressure increases. This effect cannot be understood from the hydrodynamic point-of-view but is instead related to the nonlocal character of the EDF.**

***Index Terms*— nonlocal electron kinetics, positive column of glow DC discharge, electron distribution function.**

I. Introduction

When simulating gas-discharge plasmas, the electron distribution function (EDF) is usually calculated using the traditional local approximation [1], [2]. This means that terms with both spatial gradients and an ambipolar electric field are omitted in the kinetic equation and the EDF is factorized as

$$f_0(w, \mathbf{x}) = n_e(\mathbf{x}) f_0^0(w, E/p) \qquad (1)$$

In this approximation, the electron distribution over kinetic energy $w = m\,v^2/2$ at a fixed point $\mathbf{x}$ depends on the local parameters, primarily the heating electric-field intensity E and the pressure. The inhomogeneity results in small corrections which determine particle and (if necessary) energy fluxes, which are proportional to the relatively small gradients of these parameters. They manifest themselves in the formation of fluxes of particles and energy, which are proportional to these gradients. Such an approach is characteristic for the so-called fluid approach, see for example [1], [2], [3]. In this approximation, the direction of the differential fluxes, i.e. of the contributions of different EDF parts to the total particle and energy fluxes, coincides with the directions of the total fluxes. Correspondingly, the rates of electron collisions, i.e. impact excitation rates

$$W_k(\mathbf{x}) = 4\pi \int_{v_k}^{\infty} f_0(v, \mathbf{x}) \nu_k(v)\, v^2 dv = \nu_k(E/p) n_e(\mathbf{x}) \qquad (2)$$

(where $v_k = \sqrt{2\varepsilon_k/m}$) of atomic energy levels k with threshold energy ε_k, are proportional to the electron density $n_e(\mathbf{x})$ [1], [2]. These rates control plasma-chemical reaction rates, plasma luminosity and composition, ionization, etc. Thus, the excitation frequencies, $\nu_k(E/p)$, are determined by the local EDF, f_0^0, which depends on the local values of the heating electric-field intensity and other parameters (the gas temperature, the density of excited particles, etc.). Consequently, in the gas-discharge plasmas this field is the dominant factor which controls spatial W_k profiles, and they are expected to reproduce the heating field and the electron density profiles. Therefore in a DC positive column plasmas, where electrons are heated by the uniform longitudinal electric field E_z, the common expectation is that all the excitation rates in a column are maximal on the tube axis, where the plasma density is maximal. Nevertheless, in simulations [4], [5] of the positive column (PC) in Argon at $pR = (6-100)\, cm \cdot Torr$ (where p is pressure and R is tube radius), a surprising phenomenon was revealed, that excitation rates were maximal not on the tube axis, but shifted towards the wall. Hence, the applicability of local approximation for EDF calculations requires careful inspection.

The traditional local approach is applicable only when terms with spatial gradients are small and can be omitted in the kinetic equation, i.e. when electron energy relaxation length λ_ε is significantly less then size of spatial inhomogeniety of plasma [6]. In the opposite case the nature of EDF is nonlocal, i.e., its value at a given point depends on the distribution of the physical parameters (primarily on the electric field strength) within the sphere with center placed in a given point and with radius λ_ε, rather than on their local values. Estimating λ_ε one must take into account that the relation between the volume processes and the diffusion of electrons to the walls could be different for different electron energy ranges.

If the electron energy balance is determined by elastic collisions, then for atomic gases in the energy range $\varepsilon < \varepsilon_1$ (where ε_1 is inelastic processes threshold energy) in which most electrons are concentrated, the electron energy relaxation length is

$$\lambda_\varepsilon \simeq \sqrt{D_x/(\delta\nu)} \simeq \lambda/\sqrt{\delta} > 100\lambda \qquad (3)$$

(where λ is the electron mean free path, $D_x = \lambda v/3$ is the coefficient of spatial electron diffusion and $\delta = 2m/M$). When $\lambda_\varepsilon > \Lambda$ (where Λ is characteristic diffusion length), the EDF is nonlocal throughout the whole plasma volume. The length (3) is more than two orders of magnitude larger than the electron

E.A.Bogdanov is with Vavilov State Optical Institute, St.Petersburg, 199034 Russia Email: eugene72@mail.ru

A.A.Kudryavtsev is with St. Petersburg State University, St. Petersburg, 198504 Russia Email: akud@ak2138.spb.edu

L.D.Tsendin is with St. Petersburg State Polytechnic University,St. Petersburg, 195251 Russia Email: tsendin@phtf.stu.neva.ru

mean-free-path, and the inequality $\lambda_\varepsilon > \Lambda$ is satisfied up to relatively high pressures $p \cdot \Lambda \leqslant (5-10)$ cm·Torr.

Since at $\lambda_\varepsilon > \Lambda$ the energy of an electron changes only slightly during its single pass across the discharge volume, the total energy

$$\varepsilon = w + e\varphi(\mathbf{x}) = m\,v^2/2 + e\varphi(\mathbf{x}) \tag{4}$$

(the kinetic energy plus the potential energy) is the integral of motion of such electrons.

In the energy range $\varepsilon > \varepsilon_1$, which corresponds to inelastic collisions, an electron diffuses in the electron energy relaxation length λ_ε^* before inelastic collision occurs:

$$\lambda_\varepsilon^* = \sqrt{D_x/\nu_1} \simeq \sqrt{\lambda\lambda^*} \simeq (3-10)\lambda \tag{5}$$

(where, $\lambda^* = 1/(N\sigma^*)$ is the electron mean-free-path for inelastic processes and ν_1 is frequency of inelastic collisions) and its characteristic lifetime is $1/\nu_1$. The length λ_ε^* (5) is much shorter than λ_ε that is given by Eq. (3).

Therefore, from the physical standpoint, the most convenient variables for describing a nonlocal EDF are the variables ε and $\mathbf{x}$ [3], [6]. Because of the presence of two very different energy scales, the nonlocal character of the EDF manifests itself in different ways in its different parts. In terms of the total energy (4), the nonlocal EDF can be either dependent on, or independent of, the spatial coordinate $\mathbf{x}$ [6]. The most examined marginal case of low pressures when $\lambda_\varepsilon^* > \Lambda$ and the EDF at $\varepsilon \leqslant e\Phi_w$ depends only on the total energy ε [6], [7], [8] (Φ_w is the potential difference between the discharge axis and the tube wall). At higher pressure, when the inequality $\lambda_\varepsilon > \Lambda > \lambda_\varepsilon^*$ holds, the situation becomes more diverse [4], [9], [10]. In this case the bulk of the EDF at $\varepsilon < \varepsilon_1$ remains a function of ε only, but the EDF tail, at $\varepsilon > \varepsilon_1$, depends both on ε and $\mathbf{x}$. The analysis of this case was started only recently [4], [5], [9], [10], [11] and many surprising phenomena were discovered. One of the most impressive is the case of paradoxical non-monotonic behavior of excitation-rate spatial profiles in DC positive column (PC) plasmas [4], [5], [11].

In this paper we present the main results, their concise explanation, and scalings for the excitation profiles in a PC at moderate and high pressures.

II. Numerical simulations results in Positive Column

The positive column (PC) plasma is the most studied object of the low-temperature plasma physics. The relative simplicity of its creation and diagnostics makes it traditional benchmark and testing field for many novel concepts and approaches. It was pointed out in [4], [5] that the above-mentioned paradoxical phenomenon of non-monotonic behavior of excitation-rate spatial profiles are caused by the non-local electron kinetics [6], and in [11] was presented a kinetic analysis of the problem.

The simulation code used in this work is described in detail in [12]. The code solves equations of continuity for plasma species and Poisson equation for the electrostatic field. Heavy particles were described by a fluid model. The electron distribution function is calculated by solving the Boltzmann equation using a two-term spherical harmonics expansion. For EDF calculations, we have accounted for various processes including stepwise excitation and ionization, as well as the generation of energetic electrons in superelastic collisions with metastables and Penning ionization between metastables. At the tube wall $r = R = 1$cm, the loss-cone boundary condition has been used (see e.g., [8], [9]). We consider six plasma species: Ar (ground state), Ar^* (metastable state) with energy ε_1=11.55 eV, Ar_r^* (resonance state, 11.73 eV), Ar^{**} (13.2 eV), Ar^+, and Ar_2^+ (atomic and molecular ions). The argon chemistry mechanism is similar to that used in [5] (see also [13] with similar mechanism for xenon). It includes conversion of the atomic to molecular ions and thus could be used in a wide range of gas pressures. The mechanism consists of 21 reaction steps, including various electron-induced excitation, de-excitation, ionization steps and radiative transitions: $Ar^{**} \rightarrow Ar^*$ and $Ar_r^* \rightarrow Ar$ (radiation trapping includes both Doppler and collisional line broadening account).

The calculated radial profiles of excitation rates R_1 and R_2 for the reactions $Ar + e \leftrightarrow Ar^* + e$ and $Ar + e \leftrightarrow Ar^{**} + e$ presented in Fig. 1 for different gas pressures. Off-axis peaks of both excitation rate profiles are observed for a pressure range $5 < p < 50$ Torr. The R_2 peaks (Fig. 1b) are more pronounced than the R_1 peaks (Fig. 1a). The nonmonotonic excitation rates result in nonmonotonic distributions of excited species. For example, Fig. 2 shows the radial profiles of Ar^* density at different gas pressures. One can see that Ar^* density is nonmonotonic at pressures from 5 to 50 Torr.

The densities of other excited species have similar radial profiles. The electron density profiles are close to Bessel distributions with the maximum values varying from 1.6×10^9cm^{-3} (at 1 Torr) to 1.5×10^{10}cm^{-3} (at 100 Torr). The axial electric field E_z calculated self-consistently by the code has values 6.9, 6.2, 12.1, 31.3, 64.9, and 131.7 V/cm for p=1, 5, 10, 25, 50, and 100 Torr, for the fixed discharge current of 1 mA. For such a low current, Coulomb collisions, volume recombination, and gas heating are not important.

Thus the observed effects cannot be understood from the hydrodynamic point of view and their understanding can be achieved by analysis of electron kinetics in PC at moderate gas pressures.

III. Kinetic analysis

Let us give a kinetic analysis of the problem for the excitation profiles in a PC. In order to clarify the underlying physics, here we consider the model problem as a plane-parallel (rather then cylindrical as in the real PC) geometry with the gap spacing $2L$. This simplificatition does not lead to losing the essence of investigated phenomenon.

If independent variables are spatial coordinate x ($-L \leqslant x \leqslant L$) and the total electron energy ε (4) then the kinetic

equation takes the form (see, for example, [6], [11]):

$$\frac{\partial}{\partial x}\left(\sqrt{w}D_x\frac{\partial f_0}{\partial x}\right)+\frac{\partial}{\partial \varepsilon}\left(\sqrt{w}\left(D_E\frac{\partial f_0}{\partial \varepsilon}+V_{ea}f_0\right)\right) = \sum_k\Big(\nu_k(w)\sqrt{w}\ f_0(\varepsilon) - \nu_k(w+\varepsilon_k)\sqrt{w+\varepsilon_k}\ f_0(\varepsilon+\varepsilon_k)\Big) - \frac{N_m g_a \nu_1(w)\sqrt{w}}{N_0 g_m}\ f_0(\varepsilon-\varepsilon_1)\ . \tag{6}$$

This equation accounts for both the longitudinal E_z and perpendicular (ambipolar) $E_x=-\partial\varphi/\partial x$ electric fields. Here $D_E=(eE_z)^2D_x$ is the energy diffusion coefficient, which relates to the Joule heating by the field. The energy loss in the elastic collisions causes in the "velocity" along the energy axis $V_{ea}=w\delta\nu$. The right-hand side of Eq.(6) includes sources and sinks due to inelastic processes. Here, ν_k corresponds to the inelastic collisions with excitation of an atomic level k. The first term within the sum Σ_k is non-zero only at the EDF tail, when $w>\varepsilon_1$ (in the region III in Fig. 3a). The second one desribes the electrons appearing after an inelastic collision with small energy; it is important only at small energies (in the region I in Fig. 3a) and will be neglected at later. The last term in (6) desribes the electrons appearing after superelastic collisions $e+Ar^*\rightarrow e+Ar$ of electrons with long-living metastable atoms. In this process slow bulk electron additionally acquires the threshold excitation energy ε_1 and instantaneously becomes fast. Such processes have substantion impact on effective constants of excitation reactions with high threshold energies and, accordingly, on the densities of highly excited states (see [5] for details). ν_1 is the excitation frequency of the metastable level, N_0 and N_m are ground state and metastable atoms density and $g_a,\ g_m$ - their statistical weights.

The kinetic equation (6) is the 2D diffusion equation with ε and x, as variables. It is reasonable to introduce the differential flows along the energy axis and along the spatial coordinate x (it would be radial coordinate r in the real PC case):

$$\Gamma_\varepsilon=-\left(D_E(w,x)\frac{\partial f_0}{\partial\varepsilon}+V_{ea}(w)f_0\right) \tag{7a}$$

$$\Phi_x=-D_x(w)\frac{\partial f_0}{\partial x} \tag{7b}$$

At moderate and higher pressure, when $\lambda_\varepsilon>\Lambda>\lambda^*_\varepsilon$, as already mentioned, the bulk of the EDF at $\varepsilon<\varepsilon_1$ remains a function of ε only, but the EDF tail, at $\varepsilon>\varepsilon_1$, depends both on ε and x. When a kinetic energy $w=\varepsilon-e\varphi(x)>\varepsilon_1$ exceeds the inelastic collision threshold ε_1 (region III in Fig. 3), the EDF decreases sharply, $\sim\exp(-\varepsilon/T^*)\sim\exp(-x/\lambda^*_\varepsilon)$, where

$$T^*(\varepsilon)\simeq(D_E/\nu_1)^{1/2}=eE_z\lambda^*_\varepsilon \tag{8}$$

is the electron "temperature" in the inelastic region. The electrons with $w>\varepsilon_1+T^*$ are practically absent. In the region IIb (see Fig. 3a), inelastic collisions are absent and an intense inward-directed differential spatial flux $\Phi_x(\varepsilon,x)$ (the diffusive flux of electrons with the given total energy) is formed [9] (see Fig. 3a). At the boundary between the regions IIb and III, which is given by a relation

$$e\varphi(x_1(\varepsilon))=\varepsilon-\varepsilon_1\ , \tag{9}$$

a zero boundary condition for the EDF values ("black wall" approximation [6]) should be imposed.

If $L>>\lambda^*_\varepsilon$ the expression (2) for the total excitation rate could be considerably simplified. The differential flux Φ_x, and the flux Γ_ε along the energy axis are shown in Fig 3a. The excitations occur in the narrow ($\sim T^*$) strip in the (ε,x) plane (dotted line in Fig. 3b). Multiplying (6) by $(4\pi v^2dv\,dx)$ and integrating it over the srip, which length Δx satisfies the conditions

$$L>>\Delta x>>\lambda^*_\varepsilon\,, \tag{10}$$

we obtain an expression for the total excitation rate W_{ex}:

$$W_{ex}(x)\Delta x=-\frac{4\pi v_1}{m}\Delta x\left[\Gamma_\varepsilon+\frac{\Delta\varepsilon}{\Delta x}\frac{\partial f_0}{\partial x}\right] = -\frac{4\pi v_1}{m}\Delta x\left[D_E\frac{\partial f_0}{\partial\varepsilon}+D_x(eE_x)\frac{\partial f_0}{\partial x}\right]\ . \tag{11}$$

The first term in the expression for the excitation rate (11) corresponds to the traditional mechanism of Joule heating (the diffuson in energy). It is maximal at the gap midplane. Since the EDF in the region IIb (see Fig. 3a) decreases exponentially with energy, the corresponding contribution to the exitation rate (2) decreases towards the column periphery. The second term relates to the differential flux Φ_x that is inward-directed in the region IIb (see Fig. 3a). Its direction is determined by positive spatial gradient $\partial f_0/\partial x$ at fixed ε; the last due to sink "black wall" at the $x=x_1(\varepsilon)$ point. Since this flux corresponds to the diffusion with ε conservation, the kinetic energy of electrons in the range $\varepsilon_1<\varepsilon$ increases. In other words, these electrons are "heated" by the radial electric field. It is to be noted that in our approximation the total electron transverse flux equals zero (the flux Φ_x in region IIa is outward directed, Fig. 3a, and compensates the inward-directed flux in IIb). That is why this effect cannot be treated in the conventional terms of the fluid approximation (see [9] for details). This spatial term is proportional to

$$\Delta\varepsilon=eE_x\Delta x \tag{12}$$

and equals zero both at $x=0$ and at $x\rightarrow L$; thus the peripherically peaked profiles of $W_{ex}(x)$ arise, if this term dominates.

At $\lambda_\varepsilon>L$ the term V_ε in (6) can be neglected in the region IIb. So we have an estimate for the excitation rate profile

$$\frac{W_{ex}(x)}{W_{ex}(0)}=\Big[\frac{\partial f_0(x,\varepsilon)}{\partial\varepsilon}+\frac{E_x}{(eE_z)^2} \times\frac{\partial f_0(x,\varepsilon)}{\partial x}\Big]\Big|_{\varepsilon=e\varphi(x)+\varepsilon_1}\times\left(\frac{\partial f_0}{\partial\varepsilon}\Big|_{x=0,\,\varepsilon=\varepsilon_1}\right)^{-1} \tag{13}$$

We performed estimates of the rate profile (13) using the WKB solution for the EDF in the region IIb that was formulated in [9]. This solution satisfies zero boundary conditions for the function f_0 at $x=x_1(\varepsilon)$ (9), and for its spatial derivative at

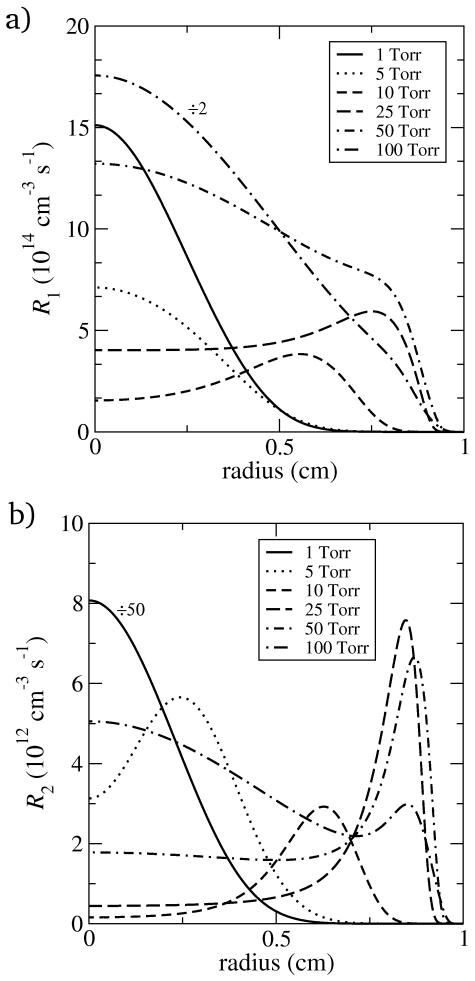

Fig. 1. Radial profiles of excitation rates of Ar^* (a) and Ar^{**} (b) at different pressures.

$x = L$, and is exponentially decreasing with ε [9]

$$f_0\left(x,\varepsilon\right) \simeq \exp\left[-\Psi(\varepsilon)\right]\,\sin\left[\frac{\pi}{2}\frac{(x-x_1(\varepsilon))}{(L-x_1(\varepsilon))}\right]\,;$$

$$\Psi(\varepsilon) = \frac{\pi}{2}\int\limits_{\varepsilon_1}^{\varepsilon}\sqrt{\frac{D_x}{D_E}}\frac{d\varepsilon'}{(L-x_1(\varepsilon))} \approx \frac{\pi}{2}\frac{(\varepsilon-\varepsilon_1)}{eE_z(L-x_1(\varepsilon))}\,. \tag{14}$$

The first term in the numerator in (13) decreases with x due to EDF decrease along the boundary between the regions III and IIb. On the contrary, the second one is zero at $x = 0$. It rises at small x values due to the $E_x(x)$ rise. At larger x values the exponential decrease of the EDF $f_0(x, \varepsilon = \varepsilon_1 + e\,\varphi(x))$ (see (14)), overcomes this factor, and so this term has a maximum at some $x \neq 0$. The estimate of (13) yields

$$\frac{W_{ex}\left(x\right)}{W_{ex}\left(0\right)} \approx \exp\left[-\frac{\pi}{2}\frac{\varphi(x)}{E_z(L-x)}\right] \times \left(1+\frac{E_x}{E_z}\right)\,. \tag{15}$$

The effect can be interpreted in terms of an electrostatic analogy (Fig. 4). Neglecting the drift term V_ε in the energy flux, the last term in the right-hand side of (6), and using the absorbing wall approximation, the problem is reduced to the Laplace equation. It can be treated as finding the electrostatic

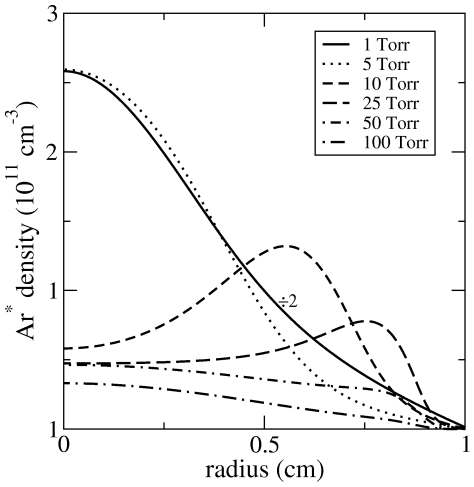

Fig. 2. Radial profiles of excited Ar^* species at different pressures.

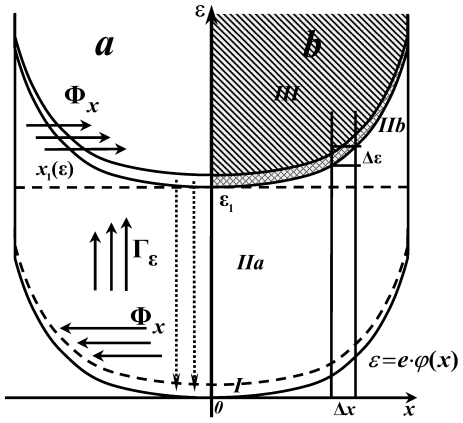

Fig. 3. **a**) Formation scheme of the spatial differential fluxes $\Phi_\varepsilon(x,\varepsilon)$, and of the flux in energy $\Gamma_\varepsilon(x,\varepsilon)$. The dashed arrows relate to the electrons which have lost energy by inelastic collisions. **b**) The integration domain of (6) in the (x,ε) plane.

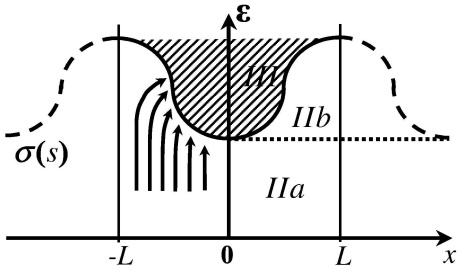

Fig. 4. Electrostatic analogy.

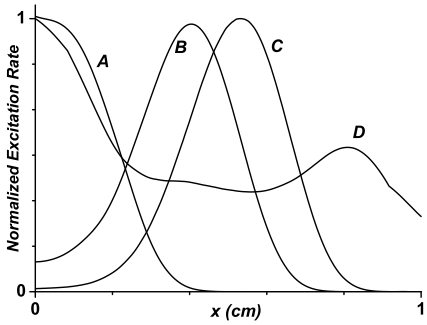

Fig. 5. Spatial profiles of the total excitation rate for E_z/p = 0.65 V/(cm·Torr) and $e\varphi(r) = \varepsilon_1(x/L)^3$ for different p=0.5(A), 5(B), 10(C) and 100(D) Torr.

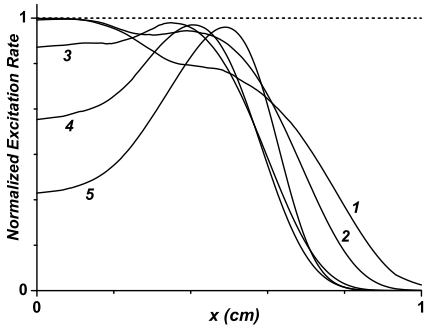

Fig. 6. Spatial profiles of the excitation rate for E_z =5 V/cm, p = 3Torr and $e\varphi(r) = \varepsilon_1(x/L)^3$ for different a = 0(dotted line), 0.25(curve 1), 1(curve 2) and 1.5(curve 3).

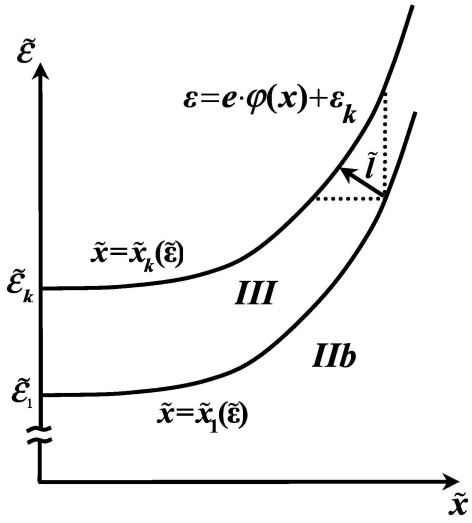

Fig. 7. Formation scheme of excitation spatial profiles for high energy levels.

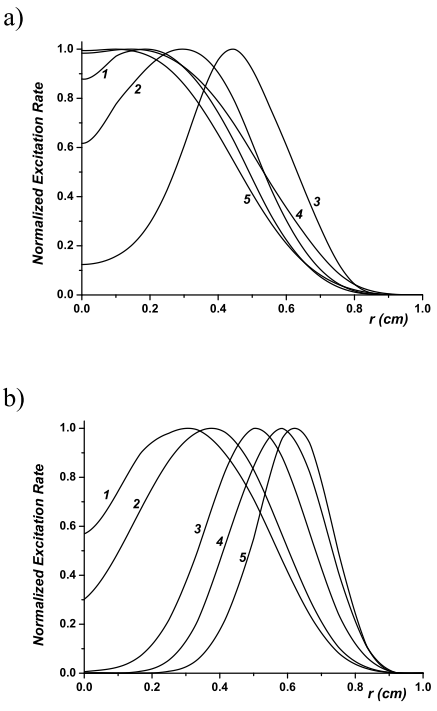

Fig. 8. Profiles of excitation rates (normalized to their maximal values) of different levels of Argon atoms k = 1 (curve 1), 3 (2), 5 (3), 17 (4) and 25 (5) with energies ε_k = 11.55, 11.72, 12.91, 14.01, 15.2 eV, respectively, calculated (a) without and (b) with allowance for superelastic collisions; r_0 is the peak coordinate of the excitation rate profile.

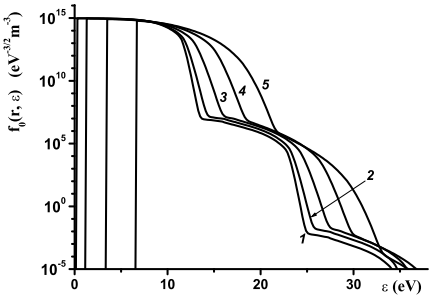

Fig. 9. EDFs at different radii r as function of the total energy ε: r = 0 (curve 1), 0.2R (2), 0.4R (3), 0.6R (4) and 0.8R (5).

"potential" of a uniformly charged plane at $\varepsilon = 0$, while the boundary between III and IIb is analogous to the conducting surface, and the excitation rate is analogous to the surface charge per unit length along the x axis $\sigma(x)$. The boundary condition of zero flux at the vessel wall can be interpreted as the periodicity condition along x. So, it is obvious that if some parts of the conducting surface are normal to x, the surface charge per unit length along the x axis tends to infinity there. On the contrary, if the conducting surface is gradual enough, the surface charge on the conductor per unit length along x is maximal at the points where ε at the conductor surface is minimal.

Let us return to our model problem. If the ambipolar

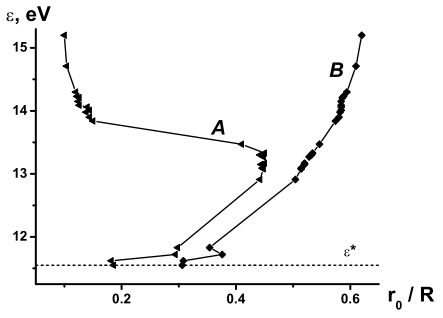

Fig. 10. The peak coordinate r_0 of the excitation rate profile for the k-th level as a function of the energy ε_k of this level. Curves A and B show the results of calculations with and without allowance for the superelastic collisions, respectively. The dotted line corresponds to the energy of the metastable state.

potential is approximated as

$$e\,\varphi(x) = -a\,\varepsilon_1 (x/L)^n/n \tag{16}$$

it is easy to derive the algebraic equation for the maximum $W_{ex}\,(x)$ position x_0 of (15). If $A = \varepsilon_1/(eE_zL) \gg 1$ then the value of x_0 can be estimated as:

$$x_0 = \sqrt[n]{n/(\pi A a)} \tag{17}$$

The formulated considerations are illustrated for the model problem in the slab (plane-parallel) geometry with $2L$=2 cm. For $\varphi(x)$ we had used approximation (16) with n =2 and 3. The spatial profiles of the excitation rate $W_{ex}(x)$ (2) are presented in Fig. 5 for $E_z/p = const$ and different pressures p [11]. It could be seen that at low pressure, when the whole EDF is nonlocal, the total excitation rate is peaked at the plasma center (curve A). In contrast, at moderate pressure the peak of the $W_{ex}(x)$ (curves B, C) is substantially displaced from the PC axis. The x_0 positions for curves B and C obtained from (16), (17) are 0.33 and 0.38 accordingly; These values are in agreement with numerical results (Fig. 4): 0.41 and 0.55. At higher pL it holds $\lambda_\varepsilon < L$, and the EDF in the central part of region II becomes local. Nevertheless, nonlocal effects still exist at a distance λ_ε from the wall, if the potential profile $\varphi(x)$ in the wall vicinity is steep enough. It can be seen from the curve D that the $W_{ex}\,(x)$ profiles in the central vessel part are maximal at $x = 0$, but at the distance from the wall of the order of λ_ε (3), where the EDF is non-local, the satellite maximum remains. If the $\varphi(x)$ profile is more gradual (say, for $n = 3/2$ in (15)), the satellite maximum disappears. A quick test for existence of nonmonotonic profiles and a maximum position gives Eq. (15). It means, in particular, that excitation profiles expected to be nonmonotonic when E_x exceeds the longitudinal field E_z. Therefore, for the effect presence the profile of radial potential should be rather steep. In Fig. 6 the excitation rate spatial profiles $W_{ex}\,(x)$ are presented in dependence of E_x value. In the absence of the transverse electric field the dependence of total excitation frequency W_{ex} is independent of x. At low E_x, W_{ex} has maximum at $x = 0$; at higher E_x, the maximum is shifted towards the periphery.

The excitation rates of individual levels $W_k\,(x)$ with the excitation energies ε_k can be divided roughly into two groups.

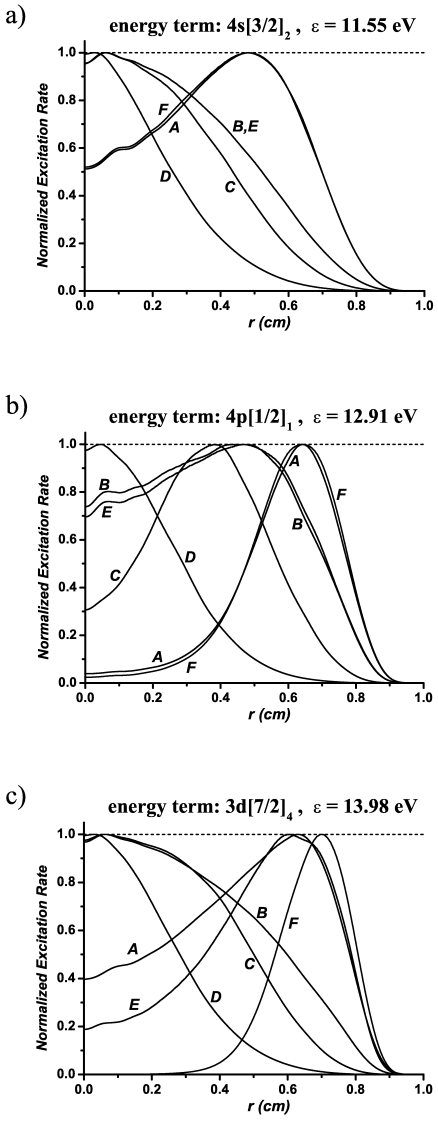

Fig. 11. Radial excitation rate profiles (normalized on maximal value) for several energy levels of Argon (with k = 1 (a), 5 (b) and 16 (c)). P = 7 Torr, R = 1 cm, I = 30 mA. A: without account of Coulomb collisions and gas heating; B: with account of Coulomb collisions, but without gas heating; C: with account of gas heating, but without Coulomb collisions; D: with account of Coulomb collisions and gas heating; E: same as B, but without account of superelastic collisions; F: without account of Coulomb collisions, gas heating and superelastic collisions.

The excitation rates for the levels with the low ε_k, for which the excitation threshold satisfies the condition $\varepsilon_k < \varepsilon_1 + T^*$, i.e., lies within the dotted strip in the Fig. 3b, the excitation rates behave, roughly speaking, in a similar way as it follows from (15). It means that shift in energy on distances less than T^* does not distort essentially the spatial profile of electon flux through the line of fixed kinetic energy ε_k, which in this case determines this excitation rate profile. The spatial profiles of the higher levels excitation rates with the threshold $\varepsilon_k > \varepsilon_1 + T^*$ (see Fig. 7) depend more on EDF behaveour in region III. Electrons in the near-axial region cannot gain energy $\varepsilon > \varepsilon_k$ in the longitudinal electric E_z field because $\varepsilon_k - \varepsilon_1 > T^*$ and

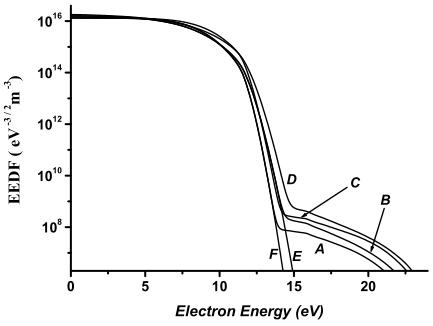

Fig. 12. EEFD on the tube axis. The sense of symbols A, B, C, D and physical conditions (P, R, I) are same as in Fig.11 (curves E and F do not presented because E almost same with B and F almost same with A).

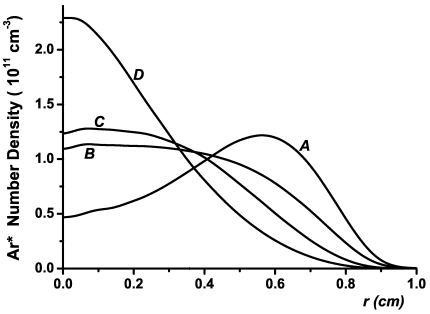

Fig. 13. The spatial profiles of metastable atoms densities. The meaning of symbols A, B, C, D and physical conditions (P, R, I) are same as in Fig.11 (curves E and F do not presented because E almost same with B and F almost same with A.).

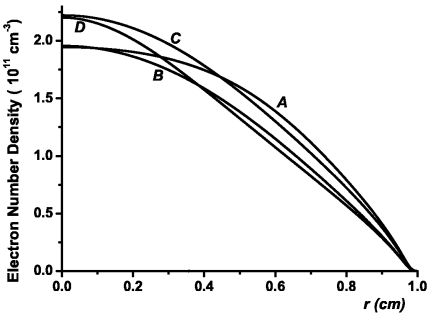

Fig. 14. Spatial profiles of electron density. The meaning of symbols A, B, C, D and physical conditions (P, R, I) are same as in Fig.11 (curves E and F do not presented because E almost same with B and F almost same with A.).

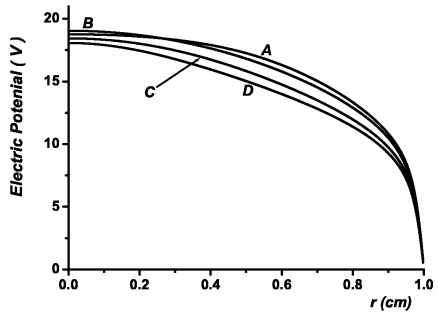

Fig. 15. The potential profiles. The meaning of symbols A, B, C, D and physical conditions (P, R, I) are same as in Fig.11 (curves E and F do not presented because E almost same with B and F almost same with A.).

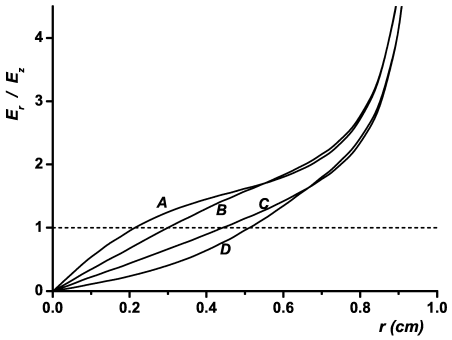

Fig. 16. Normalized to E_z profiles of radial electric field E_r. The sense of symbols A, B, C, D and physical conditions (P, R, I) are same as in Fig.11 (curves E and F do not presented because E almost same with B and F almost same with A.).

hence, they have to undergo inelastic collision before. The way by wich an electron can reach the region with $w > \varepsilon_k$ is follows: First, the electron diffuses over energy up to $\varepsilon > \varepsilon_k$ at the periphery of the plasma column, where the kinetic energy is low $\varepsilon - e\varphi(x) < \varepsilon_1$ and the electron does not undergoes inelastic collisions. Then, this electron diffuses in the radial direction toward the axis over a distance $\sim \lambda_\varepsilon^*$. For this reason, the maximum of excitation rate (and the corresponding rate constant) of the level ε_k is shifted from the curve $x = x_k(\varepsilon)$ (where $x_k(\varepsilon)$ defined by relation: $\varepsilon - e\varphi(x_k(\varepsilon)) = \varepsilon_k$) on distance λ_ε^* toward the axis.

The values of $W_k(x)$ depend most crucially on the exponentially small probability to overcome the absorbing region between the curves $\tilde{x}_1(\tilde{\varepsilon})$ and $\tilde{x}_k(\tilde{\varepsilon})$ in Fig. 7, where introduced the dimensionless units:

$$\begin{aligned} \tilde{x} &= x\sqrt{\nu_1/D_x} = x/\lambda_\varepsilon^* , \\ \tilde{\varepsilon} &= \varepsilon\sqrt{\nu_1/D_E} = \varepsilon/T^* , \end{aligned} \tag{18}$$

and $\tilde{x}_k(\tilde{\varepsilon}) = x_k(\tilde{\varepsilon}T^*)/\lambda_\varepsilon$. In order to estimate this probability, let us assume vD_x, vD_E, $v\nu_1$ to be velocity-independent. In this case we can write the kinetic equation (6) in the region III in form:

$$\frac{\partial^2 f_0}{\partial \tilde{\varepsilon}^2} + \frac{\partial^2 f_0}{\partial \tilde{x}^2} = -f_0 . \tag{19}$$

The excitation rates $W_k(\tilde{x})$ are maximal at the points where the "absorbing barrier" between the curves $\tilde{x} = \tilde{x}_1(\varepsilon)$, and $\tilde{x} =$

$\tilde{x}_k(\varepsilon)$ is most transparent. The "distance" $\tilde{l}$ between the curves $\tilde{x} = \tilde{x}_1(\varepsilon)$, and $\tilde{x} = \tilde{x}_k(\varepsilon)$ along the normal is minimal. Its "transparency" can be estimated as $\sim \exp[-\tilde{l}(\tilde{x})]$. Since the curve $\tilde{x} = \tilde{x}_k(\varepsilon)$ is shifted by $\tilde{\varepsilon}_k$ along the $\tilde{\varepsilon}$ axis in respect of $\tilde{x} = \tilde{x}_1(\varepsilon)$, this distance is maximal and equals $\tilde{\varepsilon}_k - \tilde{\varepsilon}_1$ at $\tilde{x} = 0$, and decreases monotonously from discharge center towards its periphery. For a concave potential profile of the type of (15), this rise occurs up to the distance from the wall $(L-x) \geqslant \lambda^*_\varepsilon$ where the EDF decreasing in the region IIb compensated by barrier transparency. Accordingly, the $W_k(x)$ maximum are to be rather sharp and located in the wall vicinity. It illustrates also Fig. 8a, which shows the normalized radial profiles of different Ar atoms states at p = 6 Torr, R = 1 cm, and and I = 3 mA.

IV. Discussions of spatial profiles in Positive Column

Now let us consider the results related to PC in argon simulations. In considerd conditions the destruction of metastable atoms is determined by transitions to a neighboring levels by electron impact. Due to low threshold energy of such processes, their rates almost independent on EDF form. It means that their rates can be writen in form $R_{mix} = k_{mix} n_e N_m$ where k_{mix} is constant. The balance of creation and destruction of metastable atoms in steady state is $R_{ex} = k_{mix} n_e N_m$ where R_{ex} is the excitation rate and electron density $n_e(r)$ monotonically decreases with increasing of r. Thus, in this case nonmonotonic (with shifted from axis maximum) excitation-rate profile of metastable energy level R_{ex} will lead to nonmonotonic spatial profile $N_m(r)$ of metastable atoms itself (see Fig. 2) [4], [5], [11]. With decreasing of discharge current, the destruction of metastable atoms will be determined by their diffusion and their spatial profile can be monotonic even if their excitation-rate-profile is nonmonotonic.

It follows from the above discussion that the higher the level, the larger the shift of the peak of the excitation rate profile toward the periphery caused by effects of EDF nonlocality. But usually the metastable atom density N_m is fairly high and stepwise excitation could be more effective than the above-considered direct excitation from the ground state. In such situation this shift is superimposed by the not widely known effect of the replication of the slow (nonlocal) part of the EDF in its fast part [4]. In a superelastic collisions with metastable atoms, a slow (bulk) electron participating in the reaction $Ar^* + e \rightarrow Ar + \vec{e}$ additionally acquires the threshold excitation energy ε_1 and instantaneously becomes fast. These processes substantially enhance population of the fast component of the EDF and influence on the calculated values of the constants for the excitation reactions with high threshold energies and, accordingly, the densities of highly excited states, as it illustrates Fig. 9 (see [4] for details). As it was shown in [4] and also can be seen from Fig. 9, the fast components of the EDF ($\varepsilon > \varepsilon_1$) can be represented as a sum $f_0 = f_{0t} + f_{0h}$. If the density N_m of metastable atoms is high enough, the part of the EDF which corresponds to $N_m = 0$ and sharply decreases at energies above the threshold energy ($\varepsilon > \varepsilon_1$),

$$f_{0t}(\varepsilon) \simeq c_{nt} \exp(-\varepsilon / T^*) \tag{20}$$

is supplemented with a gently sloping pedestal

$$f_{oh}(\varepsilon) \simeq \frac{N_m g_a}{N_0 g_m} f_0(\varepsilon - \varepsilon_1) \tag{21}$$

replicating the shape of the slow component (the bulk) of the EDF. Because of the low effective temperature of the fast electrons T^* (8), the EDF f_{0t} (20) falls rapidly at higher energies and, as early as at energies of a few electronvolts above the threshold ε_1, it is considerably less than the EDF f_{oh} (21) (Fig. 9). Thus, the excitation rate of higher levels can be given by sum of two terms

$$W_k(x) = W_k^t(x) + W_k^h(x) \tag{22}$$

where W_k^t and W_k^h determined by f_{0t} and f_{0h} correspondingly.

Since the energy dependence of f_{oh} is close to that of the EDF of slow electrons ($\varepsilon < \varepsilon_1$), the spatial profiles of the frequencies and rates of the processes that are determined by these parts of the EDF can also be close to one another [4]. Therefore, when the density N_m is fairly high, the maximum shift for high energy levels is superimposed by the effect of the replication of the slow (nonlocal) part of the EDF in its fast part (see [4] and Fig. 8b). Therefore, for energies $\varepsilon > \varepsilon_h$, at which the EDF f_{0h} (21) is larger than f_{0t} (20), the effect of the shift of the peak of the excitation rate profile disappears. In this case, the spatial profiles of direct ($e + Ar \rightarrow 2e + Ar^+$) and stepwise ($e + Ar^* \rightarrow 2e + Ar^+$) ionizations: $W_i^d(r)$ and $W_i^{st}(r)$ turned out similar. It can be shown in the following way. Replacing variable v within integral in (2) by $u = mv^2/2$, we can write the expressions for rates of direct and stepwise ionizations in the form:

$$\begin{aligned} W_i^d &= \frac{8\pi N_0}{m^2} \int\limits_{\varepsilon_i}^{\infty} f_0(u)\, \sigma_i(u)\, u\, du\ , \\ W_i^{st} &= \frac{8\pi N_m}{m^2} \int\limits_{\varepsilon_i - \varepsilon_1}^{\infty} f_0(u)\, \sigma_{st}(u)\, u\, du\ , \end{aligned} \tag{23}$$

where σ_i and σ_{st} are cross-sections of these processes. Because ε_i far exceeds ε_1, the f_0 in expression for $W_i^d(r)$ can be replaced by f_{0h} (21). Further, replacing of dummy variable u by $w = u - \varepsilon_1$ yields the expression for $W_i^d(r)$:

$$W_i^d = \frac{8\pi N_m g_a}{m^2 g_m} \int\limits_{\varepsilon_i - \varepsilon_1}^{\infty} f_0(r, w)\, \sigma_i(w + \varepsilon_1)\, (w + \varepsilon_1)\, dw\ . \tag{24}$$

Now the integrals in $W_i^d(r)$ and $W_i^{st}(r)$ have same lower limit $\varepsilon_i - \varepsilon_1$. The values of these integrals are determined by the integrand behaviour in thin bound of 2-3 eV at the lower limit, where the factors $\sigma_{st}(w) \cdot w$ and $\sigma_i(w + \varepsilon_1) \cdot (w + \varepsilon_1)$ can be approximated by linear functions that equal zero at $\varepsilon_i - \varepsilon_1$. So, radial dependence $W_i^d(r)$ and $W_i^{st}(r)$ turned out the same. The excitation rate radial profiles of close to ionization threshold ε_i energy levels also will be close to $W_i^{st}(r)$ profile. This is illustrated by Fig. 8b. For comparison, Fig. 10 demonstrates the position of the coordinate r_0 corresponding to the peak of the excitation rate profile for the k-th level as a function of the energy ε_k of this level. The

EDF was calculated with (curve A) and without (curve B) allowance for superelastic impacts. It can be seen that curve B increases monotonically, while in curve A the effect of shift of maximum-position is disappeared for high energy levels because the excitation spatial profiles start to repeat the profile of stepwise ionization. In other words, two parts of excitation (22) gives two different reasons of behaviour of excitation-rate profiles, which are superimposed on each other (compare the curves A and F in Fig. 11).

In a real situation, some additional affecting factors which were not accounted in kinetic equation (6) can mask the presented effects caused by EDF nonlocality. With increasing the discharge current the influence of gas heating should be expected, that results in decreasing of normal atoms density on discharge axis area. The current rise leads also to EDF maxwellization due to electron-electron collisions. To illustrate their influence, on Figs. 11-15 shown the simulation results at p = 7 Torr, R = 1 cm and I = 30 mA for different excitation energy are shown: 11.55 eV (a), 12.91 eV (b) and 13.98 eV (c). Fig. 11a corresponds to metastable level, Fig. 11b, corresponds to the intermediate excited state and Fig. 11c corresponds to the high (close to ionization threshold) energy level. The changing of corresponding EDF and the profiles of metastable atom densities are presented on Figs. 12 and 13. In accordance with previous remarks, superelastic collisions do not affect the maximum W_{ex} position of metastable states (see Fig. 11a, curves A, F), whereas they influence the maximum position of high-energy levels (Fig. 11c, curves A, F).

With electron-electron collisions included (curves B on Figs. 11-16), the nonmonotonity effect disappears for low excited levels (see Fig. 11a, curves B and E). The qualititative explanation of such an effect lies in spatial non-uniform EDF maxwellization. The maxwellization of EDF results in the depletion of the EDF bulk and in enrichment of its tail due to energy exchange between fast and slow electerons in Coulomb collisions. This influence is determined by the rate of Coulomb collisions, that is proportional to square of electron number density. Hence, this maxwellization is maximal on the disharge axis and significantly lower at its periphery. It is possible to write $f_0 = f_{00} + \tilde{f}_0$ for EDF, where f_{00} is EDF calculated for given values of field E_z, potential $\varphi(r)$ and current I without account of electron-electron collisions and $\tilde{f}_0$ is correction caused by their account. It allows to divide the excitation rates W_k on two parts W_k^0 and $\tilde{W}_k$, conditioned by f_{00} and $\tilde{f}_0$ correspondingly. The "magnitude" of $\tilde{f}_0$ (for instance, the value of $\tilde{f}_0$ at fixed kinetic energy $w = \varepsilon_1$) expected to be maximal where the rate of Coulomb collisions (which is $\sim n_e^2$) is maximal, i.e. on the axis. Thus, the part $\tilde{W}_k$ has maximum on discharge axis, whereas the radial profile of W_k^0 is nonmonotonic. For low energy levels, which close to excitation threshold, the parts W_k^0 and $\tilde{W}_k$ are comparable and their sum turned out monotonic. On the other hand, the nonmonotonic profiles of excitation rates of high energy levels (with threshold energy $\varepsilon_k > \varepsilon_1 + T^*$) are formed in a different way (see the discussion above). As a result, the nonmonotonic excitation rate profiles can remain even with account of Coulomb collisions. In self-consistent simulations the distortion of excitation profiles due to electron-electron collisions leads to modification of metastable atoms, electron density and electric potential profiles (see Figs. 13-15), and, as consequence, to reduction of the ambipolar field (see Fig. 16) and to rise of the EDF tail (see Fig. 12).

When effects of both Coulomb collisions and EDF replication (22) are accounted for, nonmonotonic excitation profiles appear only for intermediate energy levels (see Fig. 11, curve B): for the low energy levels the nomnonotonic profiles are destroyed by Coulomb collisions, and for high ones by EDF replication. Gas heating results in a nonuniform temperature profile with a maximum on axis. Due to the ideal gas law, it decreases the normal atoms density in the central part of the discharge. As the parameter E/N increases here, the diffusion in energy coefficient D_E increases in the central part of discharge volume, too. A rise of the energy and length scales (8) and (5) also plays a destructive role for the existence of nonmonotonic excitation profiles (see Fig. 11, curves C and D). In fact, gas heating and Coulomb collisions lead to an increasing the density of fast electrons on the axis that is greater than near the wall. The summary influence of both effects at hgher discharge currents will result in monotonic excitation profiles for all energy levels.

V. Conclusion

In complex systems, such as molecular gases, gas mixtures, DC and RF discharges of complex geometry and discharges in magnetic field, more complex scenaria of kinetic formation of excitation rates are expected. These relate also to the plasma luminosity and plasma composition spatial profiles.

In summary, the impact of the nonlocal character of the EDF on the spatial profiles of excitation rates is important. A paradoxical effect of non-monotonic excitation rate profiles is presented and its concise explaination is given. The related effects in a moderate and high pressure PC in Argon are considered.

Appendix

The values of longitudinal electric field E_z corresponding to Fig. 11-16 are:

No.	A	B	C	D	E	F
E_z (V/cm)	8.19	8.02	6.34	6.07	8.02	8.21

ACKNOWLEGEMENTS

The work was supported by the ISTC grant #3098. Authors also are grateful to R.R.Arslanbekov and V.I.Kolobov for numerous useful discussions.

References

[1] M. Lieberman, A. Lichtenberg, *"Principles of Plasma Discharges and Materials Processing"*, NY: Wiley, "2005.

[2] Y.P. Raizer, *"Gas Discharge Physics"*, Springer-Verlag,Berlin, Germany, 1991.

[3] E.M. Lifshitz, L.P. Pitaevsky, *"Physical Kinetics"*, Pergamon Press, Oxford, 1981.

[4] E. A. Bogdanov, A. A. Kudryavtsev, L. D. Tsendin, R. R. Arslanbekov, V. I. Kolobov, and V. V. Kudryavtsev, *"The Influence of Metastable Atoms and the Effect of the Nonlocal Character of the Electron Distribution on the Characteristics of the Positive Column in argon Disharge"*, Technical Physics, Vol. 49, No. 6, 2004, pp. 698-706.

[5] R. R. Arslanbekov, V. I. Kolobov, E. A. Bogdanov, A. A. Kudryavtsev. *"Nonmonotinic excitation rates in argon positive column",* Appl.Phys.Lett., v.85, N16, p. 33963398, 2004.
[6] L.D.Tsendin, *"Electron kinetics in non-uniform glow discharge plasmas"*. Plasma Sources, Sci. Technol., v.4, p. 200-211, 1995.
[7] J.Behnke, Yu.Golobovsky, S.U.Nisimov and I.A.Porokhova, *"Self-Consistent Model of a Positive Column in an Inert Gas Discharge at Low Pressures and Small Currents"*. Contrib.Plasma.Phys, v.36, p.75-91, 1996.
[8] U. Kortshagen, G.J. Parker and J.E. Lowler, *"Comparision of Monte Carlo simulations and nonlocal calculations of the electron distribution function in a positive column plasma",* Phys. Rev.E, v.54, p.6746-6761, 1996.
[9] G.Mumken, H.Shlueter and L.D.Tsendin, *"Formation mechanisms of radial electron fluxes in a positive column",* Phys. Rev.E., v.60, p.2250-2259, 1999.
[10] E.A.Bogdanov, A.A.Kudryavtsev, L.D.Tsendin, R.R.Arslanbekov and V.I.Kolobov, *"Nonlocal Phenomena in the Positive Collumn of a Medium-Pressure Glow Disharge",* Technical Physics, v.49, No. 7, p. 849-857, 2004.
[11] L.D.Tsendin, E.A.Bogdanov and A.A.Kudryavtsev, *"Parodoxal Non-monotonic Behaviour of Excitation-Rate Spatial Profiles in Bounded Plasmas",* Physical Review Letters, v.94, N1, 2005.
[12] http://www.cfdrc.com/∼cfdplasma
[13] E.A.Bogdanov, A.A.Kudryavtsev, R.R.Arslanbekov and V.I.Kolobov. *"Simulation of pulsed dielectric barrier discharge xenon excimer lamp",* J.Phys.D:Appl.Phys., v.37, p. 2987-2995, 2004.

Evgeny Bogdanov was born in Leningrad, USSR, 24 JAN 1972. He graduated from the St.Petersburg state University in physics in 1997; Specialization: optics and plasma physics. 2001-2004: researcher in State Petersburg University 2003: Ph.D. degree. From 2004: researcher in State Optical Institute. Area of resrerch fields includes: transport phenomenas and in electronegative plasmas, electron kinetics in rare gases, high pressure dielectric barrier discharges.

Anatoly A. Kudryavtsev was born in Altai region, USSR, in 1953. He received the M.S. and Ph.D. degrees in physics from the Leningrad State University in 1976 and 1983, respectively. Since 1982 he has been working in the St.Petersburg State University, where now he is Ass.Professor in Optics Department. Dr.Kudryavtsev is an expert in the gas discharge physics and kinetic theory of plasma physics, the authors of over 100 journal articles and numerous conference presentations.

Lev D. Tsendin was born in Leningrad, USSR, in 1937. He graduated from Leningrad State University in 1959 in theoretical physics. Since 1064 he hahas been the Leningrad Polytechnical Institute (now Sankt-Petersburg State Polytechnical University). He got his Candidat in phys-math. sciences (theoretical physics) degree in 1963, and Doctor in phys.-matrh sciences (physics and chemistry of plasma) in 1982, both at Ioffe. He is professor at the Plasma Physics chair of Physical-Technical Department of Sankt-Petersburg State Polytechnical University. His principal research interests are in plasma theory, transport phenomena in plasma, plasma kinetics and gas discharges.